Predictive Cascaded Speed and Current Control for PMSM Drives With Multi-Timescale Optimization

Wencong Tu, *Student Member, IEEE*, Guangzhao Luo, *Member, IEEE*, Zhe Chen, *Member, IEEE*, Longran Cui, and Ralph Kennel, *Senior Member, IEEE*

***Abstract*—This paper proposes a predictive speed and current control with multi-timescale optimization in a cascade architecture for a permanent-magnet synchronous motor. Considering the difference of timescale characteristics for speed loop and current loop, different sampling times are assigned to the respective subsystem. In the prediction step of the conventional two-timescale system, the coupling between slow and fast sampling models is ignored and the output of the slow-sampling model at asynchronous sampling period is missing, which both weaken the prediction performance of the system. In this paper, the predictions of both slow and fast models for all the prediction instants are analyzed in detail. Besides, a linear estimation method based on virtual instants is proposed to improve the performance of the slow-sampling model for fast prediction instants. The data stream of the proposed method is designed based on the cascaded structure. The strategies are implemented on a field-programmable gate arrays taking advantages of parallel and pipeline processing techniques. Experimental results show that the proposed strategies have a better dynamic performance compared to the conventional method.**

***Index Terms*—Field-programmable gate array (FPGA), model predictive control (MPC), multi-timescale optimization (MTO), permanent-magnet synchronous motor (PMSM).**

I. Introduction

THE permanent-magnet synchronous motor (PMSM) drives are receiving more and more attention in industry applications due to their merits of high torque/power density, high

Manuscript received August 26, 2018; revised November 21, 2019 and January 8, 2019; accepted February 1, 2019. Date of publication February 5, 2019; date of current version August 29, 2019. This work was supported in part by the National Natural Science Foundation of China under Grant 51707161, in part by the Key Program for International Cooperation and Exchange Projects of Shaanxi Province under Grant 2017KW-ZD-05, in part by the Nature Science Basic Research Plan in Shaanxi Province of China (2018JQ5187), in part by the Fundamental Research Funds for the Central Universities under Grant 3102017JC06004 and Grant 31020170QD029, in part by the Young Talent fund of Association for Science and Technology in Xian, and in part by the Shaanxi Key Laboratory of Small and Special Electrical Machine and Drive Technology. Recommended for publication by Associate Editor B. Fahimi. *(Corresponding author: Guangzhao Luo.)*

W. Tu, G. Luo, Z. Chen, and L. Cui are with the School of Automation, Northwestern Polytechnical University, Xi'an 710072, China (e-mail:

which means that the period of the speed control is ten times slower than that of the current control.

In the conventional multi-timescale control, the slow-sampling model and the fast-sampling model are analyzed separately at each sampling instant. When the slow-sampling model is analyzed, the transient process of the fast-sampling model is assumed to have been finished and the steady-state value is obtained. Similarly, when the fast-sampling model is analyzed, the slow-sampling model is considered that it cannot change timely and maintains the constant output. It is obvious that the coupling between the two-timescale models in prediction step is ignored and it affects the prediction accuracy with different horizons. Besides, the prediction of slow-sampling model remains holding state at the asynchronous sampling period. This causes some information loss and also weakens the prediction performance of the fast-sampling model. At the steady-state operation, the variables of the slow-sampling model trend to be stable. The influence of coupling term and information loss is not significant. However, at the dynamic-state operation, the variables of fast and slow models change tremendously. The coupling term and information loss affect the prediction accuracy of the fast-sampling model and the system output directly. As a result, the dynamic performance is also influenced.

This paper proposes a model predictive cascaded speed and current control with multi-timescale optimization (MTO) for PMSM drives. The prediction models for speed and current are designed separately, with deadbeat solution for the external speed loop and the FCS-MPC method [22], [23] for the internal current loop. The general multi-timescale analysis is performed based on the state-space model of two-timescale subsystems. First, according to the characteristic of sampling instant in the respective system, the analysis is divided into synchronous sampling and asynchronous sampling. Second, in order to solve the coupling relationship in prediction between the two-timescale models, the predictions of both slow and fast models for all the prediction instants are analyzed in detail. To improve the accuracy of a slow-sampling model at fast prediction instants, a linear estimation method based on virtual instants is proposed in this paper. Based on the cascaded structure, the data stream of prediction sequences is designed. In addition, a compensation method of control step delay for different timescale subsystems is proposed. Finally, the proposed method is implemented in field-programmable gate arrays (FPGAs), which are one of the best candidates for the implementation of MPC [24]. The noteworthy feature of strict timing constraints of an FPGA is exploited for multi-timescale coordinated control. The effectiveness of the proposed method is verified on a test bench involving a PMSM.

II. Model and Control Strategy

This section presents the analytic models for a PMSM and the power converter. Then, the cascaded predictive speed control strategy is designed for a PMSM, as shown in Fig. 1. It consists of four main stages that are described in detail in this section.

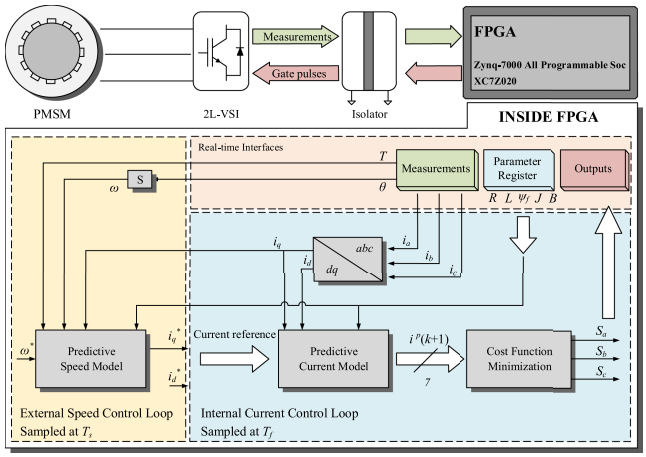

Fig. 1. Structure of predictive cascaded speed and current control for PMSM drives.

A. Model of PMSMs

The continuous-time model of a PMSM in a synchronous rotating frame can be expressed as follows:

$$u_d = Ri_d + \frac{d\psi_d}{dt} - \psi_q \omega_e \tag{1}$$

$$u_q = Ri_q + \frac{d\psi_q}{dt} + \psi_d \omega_e \tag{2}$$

$$T_e = \frac{3}{2} p \left(\psi_f i_q + \left(L_d - L_q \right) i_d i_q \right) \tag{3}$$

$$\frac{d}{dt}\omega_r = -\frac{B}{J}\omega_r + \frac{p}{J}T_e - \frac{p}{J}T_l \tag{4}$$

where $\psi_d = L_d i_d + \psi_f$ and $\psi_q = L_q i_q$ are stator d-axis and q-axis flux vectors and

u_d	direct-axis voltage;
u_q	quadrature-axis voltage;
i_d	direct-axis current;
i_q	quadrature-axis current;
ω_e	electrical angular velocity ($\omega_e = p\omega_r$);
ω_r	angular velocity;
p	number of rotor pole pairs;
ψ_f	permanent magnet flux;
R	stator resistance;
L_d	direct-axis inductance;
L_q	quadrature-axis inductance;
T_e	electrical torque;
T_l	load torque;
B	friction constant;
J	inertia constant.

B. Power Converter

The two-level voltage source inverter (2L-VSI) is applied in this paper. This converter is composed by a dc voltage source and three half-bridge units in the inverter stage. Considering that the two switches in each inverter phase operate in a complementary mode in order to avoid short circuiting the dc source, the

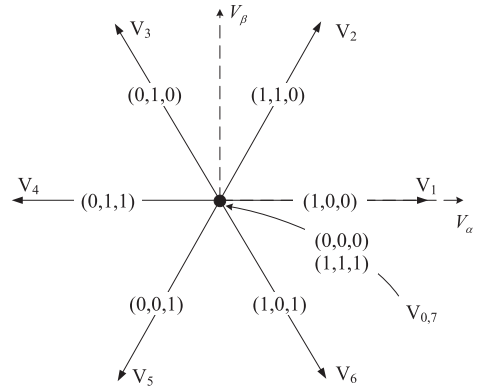

Fig. 2. Permissible voltage vectors.

switching state of the power switches can be represented by S_a, S_b, and S_c. The voltage vectors depend on the states of the converter as

$$S \triangleq \left(\frac{2}{3}\right)\left(S_a + e^{\frac{j2\pi}{3}} S_b + e^{\frac{j4\pi}{3}} S_c\right) \tag{5}$$

$$V = S \cdot V_{dc} \tag{6}$$

where V represents the output voltage vector and V_{dc} is the dc source voltage. The 2L-VSI generates eight voltage vectors, six active vectors, and two zero vectors, which are represented in Fig. 2.

C. External Speed Control Loop

The objective of external speed control loop is to achieve a good tracking of the speed reference. The deadbeat speed control is used to predict the rotor speed and output the current command in this paper. The mechanical equations (3) and (4) are adopted to obtain the second-order derivative of speed. The second-order Taylor discretization of the mechanical speed is obtained as follows:

$$\omega(k+1) = \omega(k) + T_s \cdot \dot{\omega}(k) + \frac{T_s^2}{2} \cdot \ddot{\omega}(k) \tag{7}$$

where T_s is the period of the external speed control loop.

For a surface-mounted PM motor, the direct- and quadrature-axis inductances are equal. The current reference used in the internal control loop is obtained as follows:

$$\begin{aligned} x_m^*(k) &= A_m x_m(k) + B_m u_m(k) + E_m v_m(k) + F_m \\ y_m(k) &= C_m x_m(k) \end{aligned} \tag{8}$$

where $x_m^* = y_m = i_q$, $u_m = \omega_r$, $v_m = T_l$, the subscript "*m*" denotes mechanical variables and

$$A_m = -1 + \frac{BT_s}{J}, \quad B_m = \frac{4B}{3p^2\psi_f} - \frac{4J}{3p^2\psi_f T_s} - \frac{2B^2 T_s}{3Jp^2\psi_f},$$

$$E_m = \frac{4}{3p\psi_f} - \frac{2BT_s}{3Jp\psi_f}, \quad F_m = \frac{4J\omega_{\mathrm{ref}}}{3p^2\psi_f T_s}, \quad C_m = 1.$$

where T_s is the sampling interval of the external speed loop. T_l is the load torque and the general observer was reported in [13]. ω_{ref} is the speed reference that is obtained from system setting.

D. Internal Current Control Loop

The FCS model predictive current control (FCS-MPCC) is used in the internal control loop to track the direct- and quadrature-axis current references, which are generated from the external speed loop. The discrete-time model of an electric drive is necessary to predict the future evolution of the controlled output variables for a sequence of control inputs [24]. By using the Euler approximation for the stator current derivatives for a sampling time T_f, the discrete electrical state-space model is given as follows:

$$\begin{aligned} x_e(k+1) &= A_e x_e(k) + B_e u_e(k) + E_e \\ y_e(k) &= C_e x_e(k) \end{aligned} \tag{9}$$

where $x_e = y_e = [i_d,\, i_q]^T$, $u_e = [u_d,\, u_q]^T$, the subscript "*e*" denotes electrical variables, and

$$A_e = \begin{bmatrix} 1 - \dfrac{T_f R}{L} & T_f \omega_e(k) \\ -T_f \omega_e(k) & 1 - \dfrac{T_f R}{L} \end{bmatrix}, \quad B_e = \begin{bmatrix} \dfrac{T_f}{L} & 0 \\ 0 & \dfrac{T_f}{L} \end{bmatrix},$$

$$E_e = \begin{bmatrix} 0 \\ -\dfrac{T_f \omega_e(k)}{L}\psi_f \end{bmatrix}, \quad C_e = \begin{bmatrix} 1 & 0 \\ 0 & 1 \end{bmatrix}.$$

The objectives of the MPCC are summarized as follows:

1) torque by ampere optimization (the first term of cost function);
2) torque current reference tracking (the second term); and
3) current magnitude limitation (the last term).

These objectives can be expressed as the following cost function:

$$\begin{aligned} g = {} & Q_1 (i_d(k+1))^2 + Q_2 \left(i_q^* - i_q(k+1)\right)^2 \\ & + \hat{f}\left(i_d(k+1), i_q(k+1)\right) \end{aligned} \tag{10}$$

where g is the value corresponding to the voltage vector at the (k + 1)th sampling time. Q_1 and Q_2 are the weighting factors of d- and q-axis currents. i_q* is the current reference in the quadrature axis at the (k + 1)th sampling period. It is obtained from an external control loop. The nonlinear function for limiting the amplitude of the stator current is defined as follows:

$$\begin{aligned} & \hat{f}\left(i_d(k+1), i_q(k+1)\right) \\ & = \begin{cases} \infty & \text{if} \quad |i_d(k+1)| > i_{\max} \quad \text{or} \quad |i_q(k+1)| > i_{\max} \\ 0 & \text{if} \quad |i_d(k+1)| \le i_{\max} \quad \text{and} \quad |i_q(k+1)| \le i_{\max}. \end{cases} \end{aligned} \tag{11}$$

III. General Multi-Timescale Analysis

The PMSM drive system is divided into fast and slow subsystems according to the difference between mechanical and electrical time constants. The external speed loop is the slow-sampling model, and the internal current loop is the fast-sampling model. This scheme can be extended to a general

multi-timescale system including a slow model and a fast model based on their state-space model.

For a general two-timescale control system, the state-space model of two systems can be described as follows:

Slow-sampling model

$$\begin{aligned} x_s(k+1) &= A_s x_s(k) + B_s u(k) \\ y_s(k) &= C_s x_s(k). \end{aligned} \tag{12}$$

Fast-sampling model

$$\begin{aligned} x_f(k+1) &= A_f x_f(k) + B_f u(k) \\ y_f(k) &= C_f x_f(k). \end{aligned} \tag{13}$$

The subscript denotes the model: "*s*" represents the slow-sampling model and "*f*" represents the fast-sampling model. For the convenience of analyzing the coupling relationship between the two-timescale models, some parameters are defined as follows:

1) $T_s = nT_f$;;
2) P_f and P_s are the prediction horizons of the slow-sampling model and fast-sampling model, respectively;
3) $P_f \leq T_s/T_f$; and
4) *u(k)* represents the control variables of fast and slow models. It consists of the state variable at previous instant and the increments of control variables of fast and slow model at current instant, as shown in the following equation:

$$u(k) = u(k-1) + \Delta u_f(k) + \Delta u_s(k) \tag{14}$$

where $\Delta u_f(k)$ is the control increments of the fast model calculated at fast prediction instants, and $\Delta u_s(k)$ is the control increments of the slow model calculated at slow prediction instants.

Both slow-sampling model and fast-sampling model predict the future value according to the prediction horizons at each sampling instant. The timing diagram of the subsystem is shown in Fig. 3. At the *K*th sampling instant of the slow model, as shown in Fig. 3(a), the slow prediction instants are the $(K+1)$th, $(K+2)$th $\ldots$, $(K+P_s)$th instants. Similarly, at the *k*th sampling instant of the fast model, as shown in Fig. 3(b), the fast prediction instants are the $(k+1)$th, $(k+2)$th$\ldots$, $(k+P_f)$th instants.

In two-timescale system, the sampling is divided into two categories: synchronous sampling and asynchronous sampling, as shown in Fig. 4. The asynchronous sampling instants are uniformly distributed between two synchronous sampling instants.

A. Synchronous Sampling

For synchronous sampling, both slow model and fast model predict the future and output the prediction sequences. The prediction sequence calculated by the slow-sampling model affects the output of the fast-sampling model and vice versa. As a result, the control effect of the system depends on the superposition of fast-sampling model prediction and slow-sampling model prediction. All the prediction instants for both models are analyzed in detail in this section.

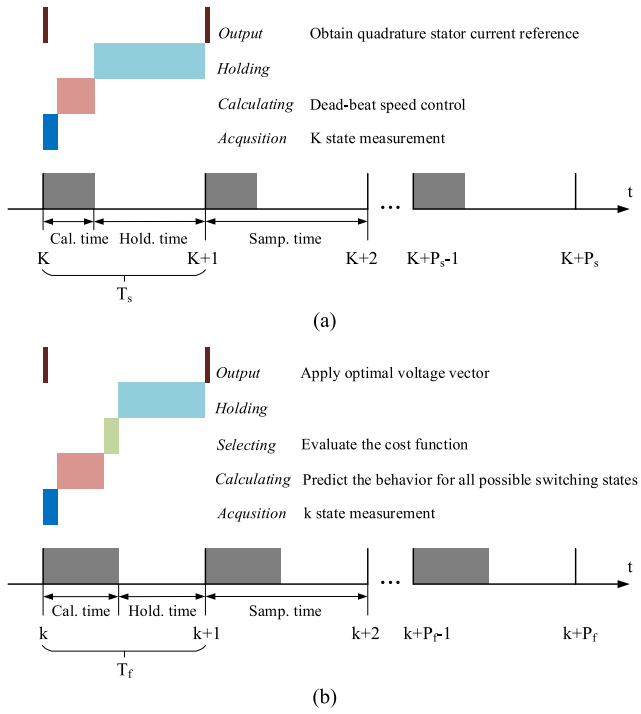

Fig. 3. Timing diagram of each subsystem. (a) Slow-sampling model. (b) Fast-sampling model.

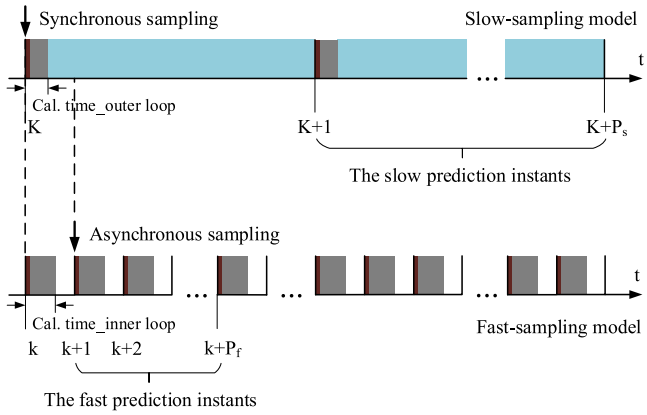

Fig. 4. Timing diagram of sampling instant in the two-timescale system.

Considering the coupling between the slow-sampling model and fast-sampling model, at the *K*th or *k*th sampling instant, the prediction sequence is divided into four categories as follows.

1) The prediction sequence $Y_s^s(K)$ of the slow-sampling model for the P_sth slow prediction instants.
2) The prediction sequence $Y_f^f(k)$ of the fast-sampling model for the P_fth fast prediction instants.
3) The prediction sequence $Y_s^f(k)$ of the slow-sampling model for the P_fth fast prediction instants.
4) The prediction sequence $Y_f^s(K)$ of the fast-sampling model for the P_sth slow prediction instants.

Y represents the prediction sequence generated by prediction models (12) and (13). The superscript denotes the

prediction instants: "*f*" represents the fast prediction instants and "*s*" represents the slow prediction instants. The subscript denotes the model: "*f*" represents the fast-sampling model and "*s*" represents the slow-sampling model.

A general cost function of the system is described as follows:

$$\min g_s = \|Y^s(k) - Y_{\text{ref }1}(k)\|^2 + \left\|Y^f(k) - Y_{\text{ref }2}(k)\right\|^2 \tag{15}$$

where $Y^s(K)$ are the predictions for the P_sth slow prediction instants and

$$Y^s(K) = \begin{bmatrix} Y_s^s(K) \\ Y_f^s(K) \end{bmatrix},$$

$$Y_s^s(K) = \begin{bmatrix} y_s^s(K+1|K) \\ y_s^s(K+2|K) \\ \vdots \\ y_s^s(K+P_s|K) \end{bmatrix},$$

$$Y_f^s(K) = \begin{bmatrix} y_f^s(K+1|K) \\ y_f^s(K+2|K) \\ \vdots \\ y_f^s(K+P_s|K) \end{bmatrix}$$

where $Y^f(k)$ are the predictions for the P_fth fast prediction instants and

$$Y^f(k) = \begin{bmatrix} Y_f^f(k) \\ Y_s^f(k) \end{bmatrix},$$

$$Y_f^f(k) = \begin{bmatrix} y_f^f(k+1|k) \\ y_f^f(k+2|k) \\ \vdots \\ y_f^f(k+P_f|k) \end{bmatrix},$$

$$Y_s^f(k) = \begin{bmatrix} y_s^f(k+1|k) \\ y_s^f(k+2|k) \\ \vdots \\ y_s^f(k+P_f|k) \end{bmatrix}.$$

$Y_{\text{ref1}}(k)$ and $Y_{\text{ref2}}(k)$ are the system references for the slow prediction instants and fast prediction instants, respectively. They are the tracking targets at each prediction instant, which are obtained from system setting or external loop command.

1) Prediction Sequence $Y_s^s(K)$ of the Slow-Sampling Model for the P_sth Slow Prediction Instants: The prediction sequence $Y_s^s(K)$ is the conventional prediction of the slow-sampling model, which is shown in Fig. 5. It is calculated by using (12) and (14) as follows, (16) shown at the bottom of this page.

$$Y_s^s(K) = \begin{bmatrix} y_s^s(K+1|K) \\ y_s^s(K+2|K) \\ \vdots \\ y_s^s(K+P_s|K) \end{bmatrix} = \underbrace{\begin{bmatrix} C_sA_s \\ C_sA_s^2 \\ \vdots \\ C_sA_s^{P_s} \end{bmatrix}}_{(S_s^s)} x_s(K) + \underbrace{\begin{bmatrix} C_sB_s \\ C_s(A_sB_s+B_s) \\ \vdots \\ C_s\sum_{i=0}^{P_s-1} A_s^iB_s \end{bmatrix}}_{(S_u^s)} u(K-1)$$

$$+ \underbrace{\begin{bmatrix} C_sB_s & & & \\ C_s(A_sB_s+B_s) & C_sB_s & & \\ \vdots & \vdots & \ddots & \\ C_s\sum_{i=0}^{M_s-1} A_s^iB_s & C_s\sum_{i=0}^{M_s-2} A_s^iB_s & \cdots & C_sB_s \\ C_s\sum_{i=0}^{M_s} A_s^iB_s & C_s\sum_{i=0}^{M_s-1} A_s^iB_s & \cdots & C_s(A_sB_s+B_s) \\ \vdots & \vdots & & \vdots \\ C_s\sum_{i=0}^{P_s-1} A_s^iB_s & C_s\sum_{i=0}^{P_s-2} A_s^iB_s & \cdots & C_s\sum_{i=0}^{P_s-M_s} A_s^iB_s \end{bmatrix}}_{(S_{\Delta u}^s)} (D_1 * U_f(K) + U_s(K)) \tag{16}$$

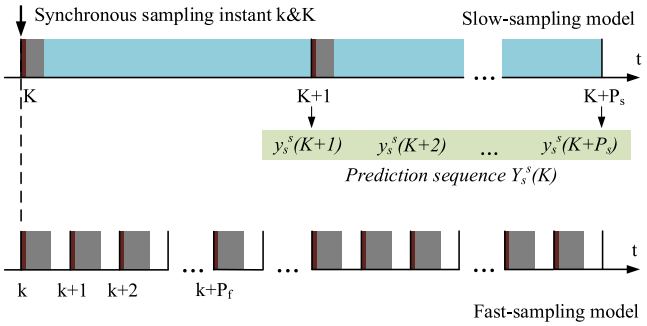

Fig. 5. Timing diagram of prediction sequence $Y_s^s(K)$.

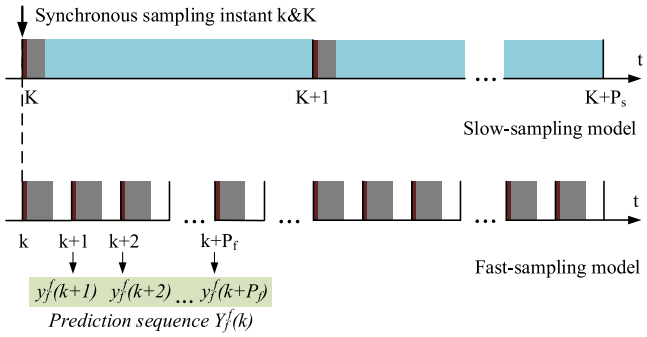

Fig. 6. Timing diagram of prediction sequence $Y_f^f(k)$.

where

$$U_f(K) = \begin{bmatrix} \Delta u_f(K|K) \\ \Delta u_f(K+1|K) \\ \vdots \\ \Delta u_f(K+M_f-1|K) \end{bmatrix},$$

$$U_s(K) = \begin{bmatrix} \Delta u_s(K|K) \\ \Delta u_s(K+1|K) \\ \vdots \\ \Delta u_s(K+M_s-1|K) \end{bmatrix},$$

$$D_1 = \begin{bmatrix} 1 & 0 & \cdots & 0 \\ 0 & \cdots & \cdots & 0 \\ \vdots & & & \vdots \\ 0 & \cdots & \cdots & 0 \end{bmatrix}_{M_s * M_f}$$

where M_s is the maximum iteration length of the slow model and when $i \geq M_s$, $\Delta u_s(K+i|K) = 0$.

Above equation can be written in the following general form:

$$\begin{aligned} &Y_s^s(K) \\ &= S_s^s x_s(K) + S_u^s u(K-1) + S_{\Delta u}^s (D_1 U_f(K) + U_s(K)) \\ &= Y_{s0}^s(K) + S_{\Delta u}^s (D_1 U_f(K) + U_s(K)). \end{aligned} \tag{17}$$

At this moment, the outputs of the slow-sampling model are affected by the control increments $U_s(K)$ and the first item $\Delta u_f(K|K)$ of the control increments $U_f(K)$.

2) Prediction Sequence $Y_f^f(k)$ of the Fast-Sampling Model for the P_fth Fast Prediction Instants: The sequence $Y_f^f(k)$ is the conventional prediction of the fast-sampling model, which is shown in Fig. 6. It is calculated by using (13) and (14) as follows, (18) shown at the bottom of this page.

$$\begin{aligned} Y_f^f(k) = \begin{bmatrix} y_f^f(k+1|k) \\ y_f^f(k+2|k) \\ \vdots \\ y_f^f(k+P_f|k) \end{bmatrix} &= \underbrace{\begin{bmatrix} C_f A_f \\ C_f A_f^2 \\ \vdots \\ C_f A_f^{P_f} \end{bmatrix}}_{\left(S_f^f\right)} x_f(k) + \underbrace{\begin{bmatrix} C_f B_f \\ C_f(A_f B_f + B_f) \\ \vdots \\ C_f \sum_{i=0}^{P_f-1} A_f^i B_f \end{bmatrix}}_{\left(S_u^f\right)} u(k-1) \\ &+ \underbrace{\begin{bmatrix} C_f B_f & & & \\ C_f(A_f B_f + B_f) & C_f B_f & & \\ \vdots & \vdots & \ddots & \\ C_f \sum_{i=0}^{M_f-1} A_f^i B_f & C_f \sum_{i=0}^{M_f-2} A_f^i B_f & \cdots & C_f B_f \\ C_f \sum_{i=0}^{M_f} A_f^i B_f & C_f \sum_{i=0}^{M_f-1} A_f^i B_f & \cdots & C_f(A_f B_f + B_f) \\ \vdots & \vdots & & \vdots \\ C_f \sum_{i=0}^{P_f-1} A_f^i B_f & C_f \sum_{i=0}^{P_f-2} A_f^i B_f & \cdots & C_f \sum_{i=0}^{P_f-M_f} A_f^i B_f \end{bmatrix}}_{\left(S_{\Delta u}^f\right)} (U_f(k) + D_2 * U_s(k)) \end{aligned} \tag{18}$$

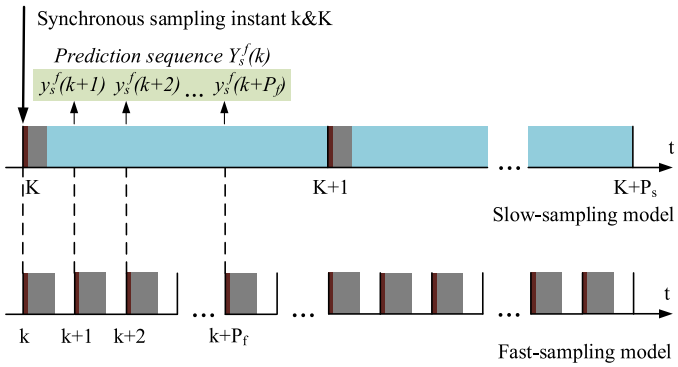

Fig. 7. Timing diagram of prediction sequence $Y_s^f(k)$.

where

$$U_f(k) = \begin{bmatrix} \Delta u_f(k\,|k) \\ \Delta u_f(k+1\,|k) \\ \vdots \\ \Delta u_f(k+M_f-1\,|k) \end{bmatrix},$$

$$U_s(k) = \begin{bmatrix} \Delta u_s(k\,|k) \\ \Delta u_s(k+1\,|k) \\ \vdots \\ \Delta u_s(k+M_s-1\,|k) \end{bmatrix},$$

$$D_2 = \begin{bmatrix} 1 & 0 & \cdots & 0 \\ 0 & \cdots & \cdots & 0 \\ \vdots & & & \vdots \\ 0 & \cdots & \cdots & 0 \end{bmatrix}_{M_f * M_s}$$

where M_f is the maximum iteration length of the fast model and when $i \geq M_f$, $\Delta u_f(k+i|k) = 0$.

Above equation can be written in the following general form:

$$\begin{aligned} Y_f^f(k) &= S_f^f x_f(k) + S_u^f u(k-1) + S_{\Delta u}^f (U_f(k) + D_2 U_s(k)) \\ &= Y_{f0}^f(k) + S_{\Delta u}^f (U_f(k) + D_2 U_s(k)). \end{aligned} \tag{19}$$

Like the slow-sampling model prediction, the outputs of the fast-sampling model are affected by the control increments $U_f(k)$ and the first item $\Delta u_s(k|k)$ of the control increments $U_s(k)$.

3) Prediction Sequence $Y_s^f(k)$ of the Slow-Sampling Model for the P_fth fast Prediction Instants: The slow-sampling model does not make prediction for the fast prediction instants ($k+1$, $k+2\ldots$, $k+P_f$), as shown in Fig. 7. Therefore, in the conventional method, the outputs of the slow-sampling model for fast prediction instants are the same, which are equal to the prediction at the *k*th instant. This paper proposes an estimation method based on virtual instants to generate the approximate prediction sequence for fast prediction instants according to the measurements and the prediction of the slow model for slow prediction instants.

At $T = 0$ instant, as shown in Fig. 8, the first prediction of the slow-sampling model at T_s instant is $y_s^s(1)$ according to (16). $y\_m_s(0)$ is the measurements of the slow model at the 0 th instant. First, a series of virtual instants in T_s period is conducted, which corresponds to the fast prediction instants. Second, a linear function is conducted to approximate the prediction sequence $y_s^f(k)$ as follows:

$$y_s^f(k) = y\_m_s(0) + \frac{k}{n}\left(y_s^s(1) - y\_m_s(0)\right). \tag{20}$$

In general, in order to use this estimation method, the prediction sequence $Y_s^s(K)$ of the slow-sampling model for the P_sth slow prediction instants should be obtained at first [see (16)]. Then, the first term $y_s^s(K+1|K)$ of prediction sequence $Y_s^s(K)$ is used in the estimation of the prediction sequence $y_s^f(k+l|k)$ of the slow-sampling model for the *l*th instants, which can be extended as follows:

$$\begin{aligned} &y_s^f(k+l\,|k) \\ &\quad = y\_m_s(K) + \frac{l}{n}\left(y_s^s(K+1\,|K) - y\_m_s(K)\right) \end{aligned} \tag{21}$$

where $l = 1, 2\ldots, P_f$, and $y\_m_s(K)$ is the measurement of the slow model at the *K*th instant.

As a result, the prediction sequence $Y_s^f(k)$ of the slow-sampling model for P_fth fast prediction instants can be derived as follows:

$$\begin{aligned} Y_s^f(k) &= \begin{bmatrix} y_s^f(k+1\,|k) \\ y_s^f(k+2\,|k) \\ \vdots \\ y_s^f(k+P_f\,|k) \end{bmatrix} = \begin{bmatrix} \frac{n-1}{n} \\ \frac{n-2}{n} \\ \vdots \\ \frac{n-P_f}{n} \end{bmatrix} y\_m_s(K) \\ &\quad + \begin{bmatrix} \frac{1}{n} \\ \frac{2}{n} \\ \vdots \\ \frac{P_f}{n} \end{bmatrix} \left(C_s A_s x_s(K) + C_s B_s u_f(K-1)\right) \\ &\quad + \begin{bmatrix} \frac{1}{n} \\ \frac{2}{n} \\ \vdots \\ \frac{P_f}{n} \end{bmatrix} C_s B_s \left(\Delta u_f(K\,|K) + \Delta u_s(K\,|K)\right). \end{aligned} \tag{22}$$

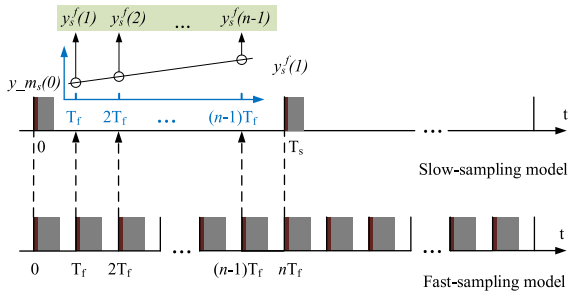

Fig. 8. Timing diagram of the proposed estimation method for prediction sequence $y_s^f(k)$.

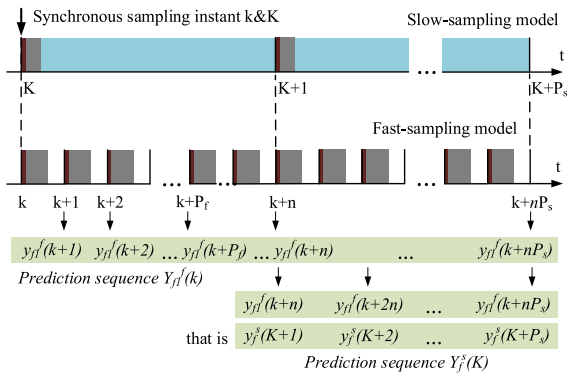

Fig. 9. Timing diagram of prediction sequence $Y_f^s(K)$.

Above equation can be written in the following general form:

$$Y_s^f(k) = Y_{s0}^f(K) + \begin{bmatrix} \frac{1}{n} \\ \frac{2}{n} \\ \vdots \\ \frac{P_f}{n} \end{bmatrix} C_s B_s \begin{bmatrix} 1 & 0 & \cdots & 0 \end{bmatrix}_{1*M_s} * \left(D_1 * U_f(K) + U_s(K)\right). \quad (23)$$

4) Prediction Sequence $Y_f^s(K)$ of the Fast-Sampling Model for the P_sth Slow Prediction Instants: The timing diagram of prediction sequence $Y_f^s(K)$ is shown in Fig. 9. The prediction sequence of the fast-sampling model for the $(P_s \times n)$th instants $Y_{f1}^f(k)$ should be obtained at first, which is given as follows:

$$Y_{f1}^f(k) = \begin{bmatrix} y_{f1}^f(k+1|k) \\ y_{f1}^f(k+2|k) \\ \vdots \\ y_{f1}^f(k+nP_s|k) \end{bmatrix}.$$

The relationship between $Y_f^s(K)$ and $Y_{f1}^f(k)$ is shown as follows:

$$Y_f^s(K) = \begin{bmatrix} y_f^s(K+1|K) \\ y_f^s(K+2|K) \\ \vdots \\ y_f^s(K+P_s|K) \end{bmatrix} = \begin{bmatrix} y_{f1}^f(k+n|k) \\ y_{f1}^f(k+2n|k) \\ \vdots \\ y_{f1}^f(k+nP_s|k) \end{bmatrix} \quad (24)$$

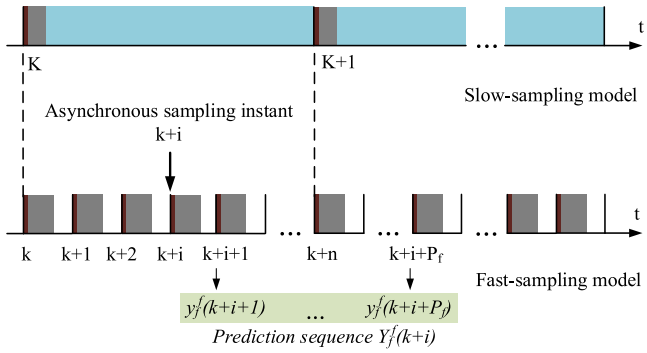

Fig. 10. Timing diagram of prediction sequence $Y_f^f(k+i)$.

Equation (25) is shown at the top of the next page.

Above equation can be written in the following general form:

$$\begin{aligned} Y_{f1}^f(k) &= S_{f1}^f x_f(k) + S_{u1}^f u(k-1) + S_{\Delta u1}^f (U_f(k) + D_2 U_s(k)) \\ &= Y_{f10}^f(k) + S_{\Delta u1}^f (U_f(k) + D_2 U_s(k)). \end{aligned} \quad (26)$$

According to the relationship in (24), the prediction sequence of the fast-sampling model for slow prediction instants can be reorganized from (26) as follows:

$$\begin{aligned} &Y_f^s(K) \\ &= S_{f2}^s x_f(K) + S_{u2}^s u(K-1) + S_{\Delta u2}^s (U_f(K) + D_2 U_s(K)) \\ &= Y_{f0}^s(K) + S_{\Delta u2}^s (U_f(K) + D_2 U_s(K)). \end{aligned} \quad (27)$$

B. Asynchronous Sampling

For the asynchronous sampling, the prediction sequences are only for the fast prediction instants as shown in Fig. 10. The control effect of the system depends on the prediction of the fast-sampling model and the estimation of the slow-sampling model.

The kth instant and the $(k+n)$th instant in the fast model are the synchronous sampling instants, as shown in Fig. 10. The $(k+1)$th, $(k+2)$th…, $(k+n-1)$th instants in the fast model are the asynchronous sampling instants. The $(k+i+1)$th, $(k+i+2)$th…, $(k+i+P_f)$th instants are termed as the fast prediction instants for the $(k+i)$th sampling instant.

Considering the coupling relationship between the slow-sampling model and fast-sampling model, the prediction sequence is divided into two categories as follows.

1) The prediction sequence $Y_f^f(k+i)$ of the fast-sampling model for the P_fth fast prediction instants.
2) The prediction sequence $Y_s^f(k+i)$ of the slow-sampling model for the P_fth fast prediction instants.

Y represents the prediction sequence generated by the prediction models (12) and (13). The superscript "f" represents fast prediction instants. The subscript denotes the model: "f" represents the fast-sampling model and "s" represents the slow-sampling model. "$k+i$" in parentheses represents the asynchronous sampling instant and $i = 1, 2 \ldots, n-1$.

$$Y_{f1}^{f}(k)=\begin{bmatrix} y_f^f\,(k+1\,|k) \\ y_f^f\,(k+2\,|k) \\ \vdots \\ y_f^f\,(k+P_f\,|k) \\ \vdots \\ y_f^f\,(k+n+1\,|k) \\ \vdots \\ y_f^f\,(k+P_s n\,|k) \end{bmatrix}=\underbrace{\begin{bmatrix} C_fA_f \\ C_fA_f^2 \\ \vdots \\ C_fA_f^{P_f} \\ \vdots \\ C_fA_f^{n+1} \\ \vdots \\ C_fA_f^{nP_s} \end{bmatrix}}_{\left(S_{f1}^{f}\right)}x_f\,(k)+\underbrace{\begin{bmatrix} C_fB_f \\ C_f(A_fB_f+B_f) \\ \vdots \\ C_f\sum_{i=0}^{P_f-1}A_f^iB_f \\ \vdots \\ C_f\sum_{i=0}^{n}A_f^iB_f \\ \vdots \\ C_f\sum_{i=0}^{nP_s-1}A_f^iB_f \end{bmatrix}}_{\left(S_{u1}^{f}\right)}u\,(k-1)$$

$$+\underbrace{\begin{bmatrix} C_fB_f & & & & & & & \\ C_f(A_fB_f+B_f) & C_fB_f & & & & & & \\ \vdots & \vdots & \ddots & & & & & \\ C_f\sum_{i=0}^{P_f-1}A_f^iB_f & C_f\sum_{i=0}^{P_f-2}A_f^iB_f & \cdots & C_fB_f & & & & \\ \vdots & \vdots & & & \ddots & & & \\ C_f\sum_{i=0}^{n}A_f^iB_f & C_f\sum_{i=0}^{n-1}A_f^iB_f & \cdots & \cdots & \cdots & C_fB_f & & \\ \vdots & \vdots & & & & & \ddots & \\ C_f\sum_{i=0}^{nP_s-1}A_f^iB_f & C_f\sum_{i=0}^{nP_s-2}A_f^iB_f & \cdots & \cdots & \cdots & \cdots & \cdots & C_fB_f \end{bmatrix}}_{(S_{\Delta u1}^{f})}(U_f(k)+D_2*U_s(k)). \tag{25}$$

The general cost function of the system is described as follows:

$$\min\, g_a=\left\|Y^f(k+i)-Y_{\mathrm{ref}}(k+i)\right\|^2 \tag{28}$$

where

$$Y^f(k+i)=\begin{bmatrix} Y_f^f\,(k+i) \\ Y_s^f\,(k+i) \end{bmatrix},$$

$$Y_f^f(k+i)=\begin{bmatrix} y_f^f\,(k+i+1\,|k+i) \\ y_f^f\,(k+i+2\,|k+i) \\ \vdots \\ y_f^f\,(k+i+P_f\,|k+i) \end{bmatrix},$$

$$Y_s^f(k+i)=\begin{bmatrix} y_s^f\,(k+i+1\,|k+i) \\ y_s^f\,(k+i+2\,|k+i) \\ \vdots \\ y_s^f\,(k+i+P_f\,|k+i) \end{bmatrix},\ i=1,2\ldots,n-1$$

where $Y^f(k+i)$ are the predictions for the P_fth fast prediction instants. $Y_{\mathrm{ref}}(k+i)$ are the system reference of the fast-sampling model and slow-sampling model.

1) Prediction Sequence $Y_f^f(k+i)$ of the Fast-Sampling Model for the P_fth Fast Prediction Instants: The sequence $Y_f^f(k+i)$ is the conventional prediction of the fast-sampling model, which is shown in Fig. 10. It is calculated by using (13) and (14) as follows, (29) shown at the top of the next page.

$$Y_f^f(k+i) = \begin{bmatrix} y_f^f(k+i+1\,|k+i) \\ y_f^f(k+i+2\,|k+i) \\ \vdots \\ y_f^f(k+i+P_f\,|k+i) \end{bmatrix} = \underbrace{\begin{bmatrix} C_f A_f \\ C_f A_f^2 \\ \vdots \\ C_f A_f^{P_f} \end{bmatrix}}_{\left(S_f^f\right)} x_f(k+i) + \underbrace{\begin{bmatrix} C_f B_f \\ C_f(A_f B_f + B_f) \\ \vdots \\ C_f \sum_{i=0}^{P_f-1} A_f^i B_f \end{bmatrix}}_{\left(S_u^f\right)} u(k+i-1)$$

$$+ \underbrace{\begin{bmatrix} C_f B_f & & & \\ C_f(A_f B_f + B_f) & C_f B_f & & \\ \vdots & \vdots & \ddots & \\ C_f \sum_{j=0}^{M_f-1} A_f^j B_f & C_f \sum_{j=0}^{M_f-2} A_f^j B_f & \cdots & C_f B_f \\ C_f \sum_{j=0}^{M_f} A_f^j B_f & C_f \sum_{j=0}^{M_f-1} A_f^j B_f & \cdots & C_f(A_f B_f + B_f) \\ \vdots & \vdots & & \vdots \\ C_f \sum_{j=0}^{P_f-1} A_f^j B_f & C_f \sum_{j=0}^{P_f-2} A_f^j B_f & \cdots & C_f \sum_{j=0}^{P_f-M_f} A_f^j B_f \end{bmatrix}}_{\left(S_{\Delta u}^f\right)} \Delta U_f(k+i) \tag{29}$$

where

$$\Delta U_f(k+i) = \begin{bmatrix} \Delta u_f(k+i\,|k+i) \\ \Delta u_f(k+i+1\,|k+i) \\ \vdots \\ \Delta u_f(k+i+M_f-1\,|k+i) \end{bmatrix}.$$

Above equation can be written in the following general form:

$$\begin{aligned} &Y_f^f(k+i) \\ &= S_f^f x_f(k+i) + S_u^f u(k+i-1) + S_{\Delta u}^f \Delta U_f(k+i) \\ &= Y_{f0}^f(k+i) + S_{\Delta u}^f \Delta U_f(k+i). \end{aligned} \tag{30}$$

2) Prediction Sequence $Y_s^f(k+i)$ of the Slow-Sampling Model for the P_fth Fast Prediction Instants: The slow-sampling model does not make prediction for the fast prediction instants ($k+i+1, k+i+2 \ldots, k+i+P_f$), as shown in Fig. 11. As previously mentioned, the estimation method that conducts a linear function to approximate the prediction sequence according to the measurements and the prediction of the slow model for slow prediction instants is proposed.

At the kth instant, as shown in Fig. 11, the first prediction of the slow-sampling model is $y_{s0}^s(K+1|K)$ according to (16). $y\_m_{s0}(K)$ is the measurements of the slow model at the Kth instant. First, a series of virtual instants are conducted, which are corresponding to the fast prediction instants. Second, a linear function is conducted to approximate the prediction

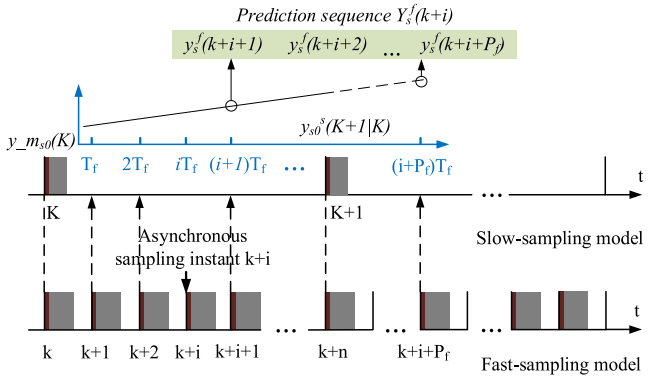

Fig. 11. Timing diagram of the proposed estimation method for prediction sequence $Y_s^f(k+i)$.

sequence $Y_s^f(k+i)$

$$\begin{aligned} &y_s^f(k+i+l\,|k+i) \\ &= y\_m_{s0}(K) + \frac{i+l}{n}\left(y_{s0}^s(K+1\,|K) - y\_m_{s0}(K)\right) \end{aligned} \tag{31}$$

where $l = 1, 2 \ldots, P_f$.

C. MPC With MTO

Based on the analysis mentioned above, the coupling between the two-timescale models in the prediction step is

TABLE I
COMPARISON BETWEEN MPC AND MPC-MTO

Sampling Condition	Prediction Sequence	MPC	MPC-MTO
Synchronous sampling	$Y_f^f(k)$	Calculated	Calculated
	$Y_s^s(K)$	Calculated	Calculated
	$Y_s^f(k)$	NO	Estimation based on virtual instants
	$Y_f^s(K)$	NO	Calculated
Asynchronous sampling	$Y_f^f(k+i)$	Calculated	Calculated
	$Y_s^f(k+i)$	NO	Estimation based on virtual instants

decomposed into several prediction sequences. The MPC-MTO is proposed in this paper, considering all the prediction sequences at specific prediction instants. Table I shows the difference between the conventional MPC and MPC-MTO. In the proposed method, the linear estimation method based on virtual instants is proposed to calculate the prediction sequence of the slow-sampling model for fast prediction instants ($Y_s^f(k)$ and $Y_s^f(k+i)$). The long horizon model prediction is performed to calculate the prediction sequence of the fast-sampling model for slow prediction instants ($Y_f^s(k)$). The complete and accurate prediction sequence is the key issue in a multi-timescale system.

In order to demonstrate the relationship among prediction sequences, the data stream of the proposed MPC-MTO is designed in Fig. 12 based on the cascaded structure. The prediction sequence of the slow-sampling model for slow prediction instants ($Y_s^s(K)$) is calculated first based on the reference with system setting. Then, the prediction sequence of the slow-sampling model for fast prediction instants ($Y_s^f(k)$ and $Y_s^f(k+i)$) is calculated, which reflects the intermediate state between two slow-sampling intants. It is the reference for the internal control loop and improves the prediction accuracy of the fast-sampling model. The system output is eventually determined by the cost function with prediction sequence of the fast-sampling model ($Y_f^f(k)$ and $Y_f^f(k+i)$) in this cascaded structure.

At steady-state operation, the variables of the slow-sampling model change less and trend to be stable. Then, the prediction sequence ($Y_s^f(k)$ and $Y_s^f(k+i)$) of the slow-sampling model for fast prediciton instants trends to be the same as prediction sequence ($Y_s^s(K)$). Hence, it has little influence on the prediction of the fast-sampling model and system output. The steady-state performances are similar for both conventional and proposed methods.

However, at the dynamic-state operation, the variables of fast and slow models change tremendously. The conventional method that lacks in the intermediate state for fast-sampling instant can only use the prediction sequence for slow-sampling instant ($Y_s^s(K)$) to do the prediction of fast-sampling model. Considering the difference in timescale between the two models, the prediction accuracy is weakened. The proposed MPC-MTO with coupling terms ($Y_s^f(k)$ and $Y_s^f(k+i)$), on the contrary, can improve the prediction accuracy of the fast-sampling model effectively. The dynamic performance is improved compared with the conventional MPC.

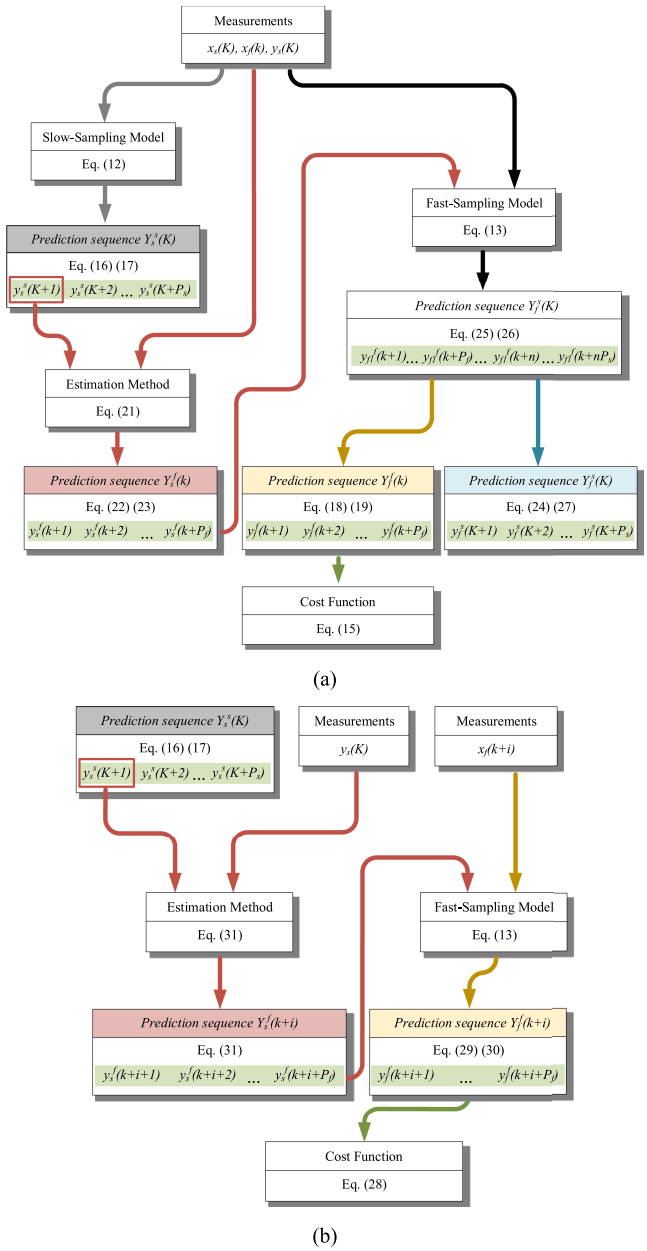

Fig. 12. Data stream of prediction sequence of the proposed MPC-MTO. (a) Synchronous sampling. (b) Asynchronous sampling.

IV. DELAY COMPENSATION

In a digital control implementation, there is a one-step inherent delay between the calculation and output, for both external speed loop and internal current loop. Based on the cascaded structure, in this paper, the cost function that determines the system output only contains the current prediction sequences.

For the internal current loop, the one-step delay usually exists between the applied voltage vector and the selected best voltage [18]. In general, the model-based two-step prediction is adopted to eliminate the side effect caused by the one-step delay [22]. The stator current at the $(k+1)$th instant is predicted first based on (10); then the predicted current $i(k+1)$ is served as the initial value to obtain the current at the $(k+2)$th instant using (10).

TABLE II
MAIN SYSTEM PARAMETERS

Control	
Sampling time for current loop T_f	50 μs
Sampling time for speed loop T_s	500 μs
FPGA frequency	50 Mhz
Prediction horizons of slow model P_s	1
Prediction horizons of fast model P_f	1
Converter	
Type	2-level VSI
DC-link Voltage Udc	270V
Dead time	2 μs
Electrical Machine	
Type	SPMSM
Rated machine speed ω_r	3000 rpm
Stator resistance R	555.22 mΩ
Rated torque T	2.3 N·m
Inductance (d axis) L_d	4.02 mH
Inductance (q axis) L_q	4.02 mH
PM rotor flux ψ_f	0.05512 V·s
Pole pairs p	5
Inertia constant J	$8.53 \cdot 10^{-5}$ kgm^2

The final cost function should be modified as follows by considering the one-step delay in practical application:

$$g' = Q_1(i_d(k+2))^2 + Q_2(i_q^* - i_q(k+2))^2 + \hat{f}(i_d(k+2), i_q(k+2)). \quad (32)$$

For the external speed loop, the one-step delay influences the outputs of current reference order. The current references with time delay are involved in the calculation of internal current loop.

According to the feature of strict timing constraints and flexible sampling time control, one optimization method designated for the implementation on an FPGA is proposed. The calculation time of speed loop in one sampling period is measurable and fixed inside the FPGA because of the pipelined parallel circuit structure. Usually, it is in nanosecond timescale and far less than sampling time of the fast model. Once the speed loop calculation is finished, the status of the slow subsystem holds, which means that the result of current reference in this control step is already uploaded in a register, waiting to be triggered. With the aid of the flexible sampling time control of an FPGA, the sampling clock of current loop can serve as the trigger to realize variable transfer from speed loop to current loop. This operation avoids the delay of data holding and the computational burden of FPGA remains the same.

V. EXPERIMENTAL RESULTS

In order to validate the performance of the developed method experimentally, an experimental setup was employed. A five-pole-pair surface-mounted PMSM is supplied by a 2L-VSI. Table II summarizes the main characteristics of the test bench. The shaft of the motor is mechanically connected to a torque transducer and a same PMSM load. The incremental encoder is fixed on the shaft to obtain the rotor position. The processor board is accompanied by a high-speed A/D interface, an incremental encoder interface, a digital output interface, and a universal asynchronous receiver/transmitter (UART) interface. The main controller board receives and processes the signals from the current and voltage transducers as well as the pulse series generated by the encoder. The circuit connection of the test bench is shown in the block diagram of Fig. 13, and Fig. 14 depicts the experimental setup used for the validation of the developed control strategy.

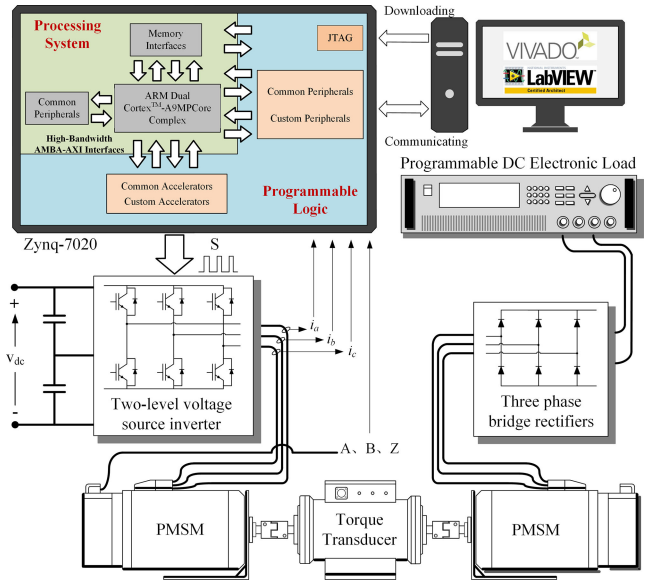

Fig. 13. Block diagram of the experimental setup.

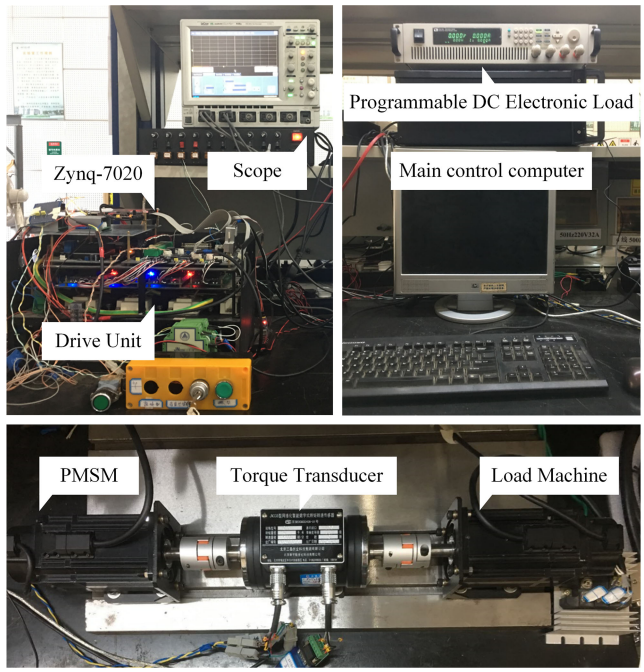

Fig. 14. Experimental setup.

The control algorithm, which is written in Verilog language, is implemented on a Xilinx Zynq (xc7z020) [25]. The CORDIC (Coordinate Rotation Digital Computer) algorithm is used for the calculation of the trigonometric and quadratic functions. The sampling time for current loop is 50 μs, whereas the speed loop runs at sampling time of 500 μs. Both conventional and pro-

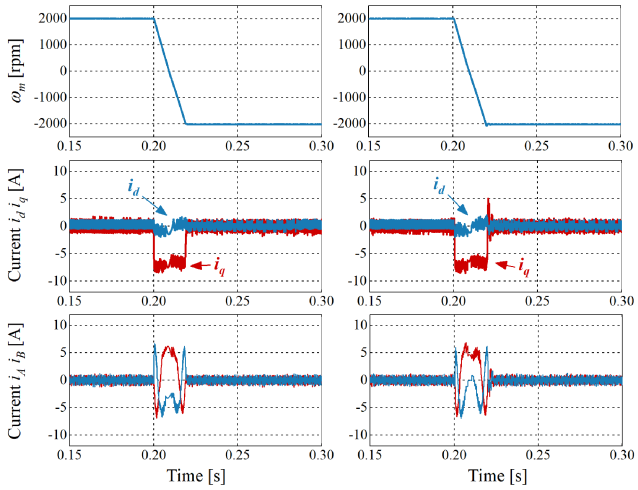

Fig. 15. Speed reversal from 2000 to –2000 r/min with no load. (a) Proposed PSC-MTO. (b) Conventional PSC.

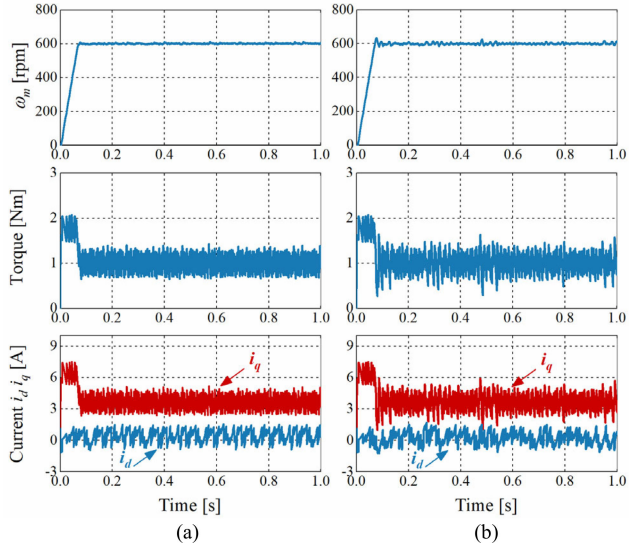

Fig. 16. Step speed change from 0 to 600 r/min with 1-N·m load torque. (a) Proposed PSC-MTO. (b) Conventional PSC.

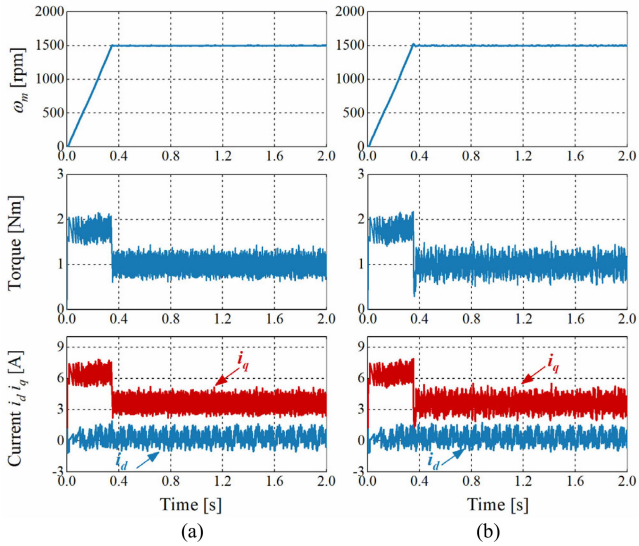

Fig. 17. Step speed change from 0 to 1500 r/min with 1-N·m load torque. (a) Proposed PSC-MTO. (b) Conventional PSC.

posed calculation algorithms are realized in a pipelined parallel architecture. Experimental test shows that the entire number of pipelined parallel steps of the proposed method is 41, which means 0.82 μs for a complete calculation. The proposed method with more computation is conducted at the cost of additional digital resources.

In this section, the developed predictive speed and current control (PSC) with MTO (PSC-MTO) is experimentally evaluated and compared with the conventional PSC [19]. The control parameters for both methods are the same, which are shown in Table II. Four different tests are performed: first, no-load speed reversal; second, speed reference change with 1 N·m load torque; third, load torque change; and fourth, steady-state operation with nominal load torque.

The performance of the proposed method is examined under speed reversal from 2000 to –2000 r/min without load torque. The purpose is to examine the dynamic speed change characteristics eliminating the impact of the load torque. Both PSC and proposed PSC-MTO exhibit the fast dynamic response, as shown in Fig. 15. The speed does not have any appreciable overshoot when the reversing maneuver is performed. However, there is a noticeable current spike of i_q with 5 A at the end of the reversing maneuver in PSC, which also results in a slight speed overshoot with 70 r/min. The proposed PSC-MTO can maintain the steady current control because of the optimization for prediction sequence with multi-timescale.

In the next step, different speed reference steps are applied to the system. The reference steps are 20%, 50%, and 90% of the rated speed with 1-N·m load. The comparison results are shown in Figs. 16–18, whereas all response characteristics are tabulated in Table III. Moreover, the torque, *dq* currents are shown. Both methods demonstrate satisfactory dynamic behavior. The *dq* currents are decoupled and both track their references fast during transient.

When the speed reference steps are applied, the tracking is dominant. Thus, the high torque is applied by the control of i_q until the speed error becomes small. When the reference steps are arrived, the lowest admissible current is applied to maintain the speed and load torque. Because of the mismatching of speed prediction and current prediction with multi-timescale, there are obvious i_q current spike and speed overshoot in PSC. Nevertheless, these are optimized in the proposed PSC-MTO. The comparisons of speed in detail are also shown in Fig. 19. The overshoot of PSC is the highest. Furthermore, compared with the proposed PSC-MTO, there are still some speed oscillations in PSC when arrived at the reference. The speed oscillation also causes the larger current ripples in this cascaded structure.

The impact of load torque is shown in Fig. 20. A load torque step 1 N·m is applied at 600 r/min. Both methods have some speed overshoot when the load torque changes, whereas the proposed PSC-MTO demonstrates a smaller overshoot with 38 r/min, compared with the conventional PSC with 51 r/min. There are also noticeable current and torque spikes in the conventional PSC, which are optimized in the proposed PSC-MTO.

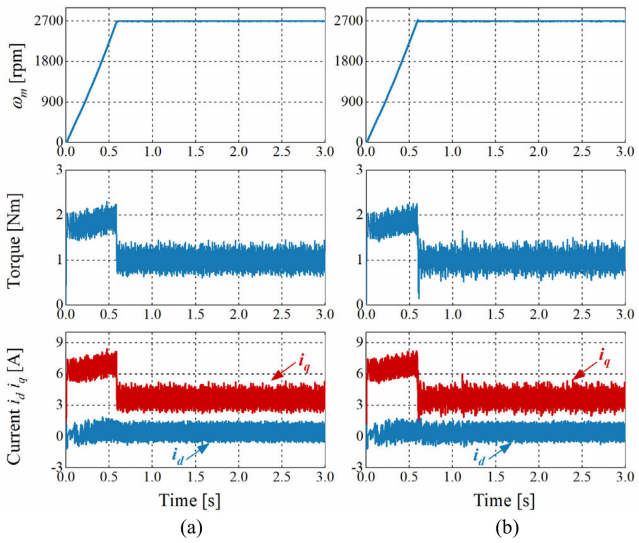

Fig. 18. Step speed change from 0 to 2700 r/min with 1-N·m load torque. (a) Proposed PSC-MTO. (b) Conventional PSC.

TABLE III
RESPONSE CHARACTERISTICS OF SPEED REFERENCE CHANGE

Parameter	Operating Condition	Conventional PSC	Proposed PSC-MTO
Speed Peak (rpm)	600 rpm	634	606
	1500 rpm	1524	1502
	2700 rpm	2722	2703
Speed Overshoot (%)	600 rpm	5.67	1
	1500 rpm	1.6	0.13
	2700 rpm	0.82	0.11
Speed Oscillation (rpm)	600 rpm	18	5
	1500 rpm	10	4
	2700 rpm	8	5
iq Current Spike (A)	600 rpm	2	0.5
	1500 rpm	2.1	0.8
	2700 rpm	2.45	0.4
iq Current Ripples (A)	600 rpm	4.4	3
	1500 rpm	3.4	3.2
	2700 rpm	4	3.3

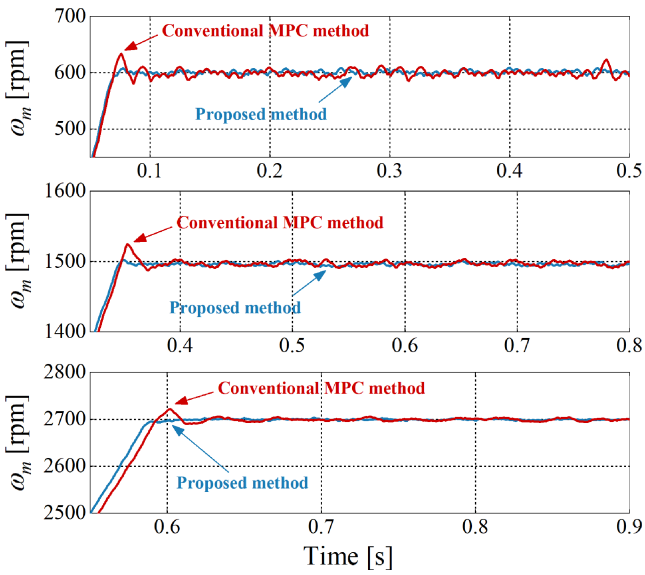

Fig. 19. Speed comparison between PSC-MTO and PSC. Zoom in the result of Figs. 16–18 (from top to bottom).

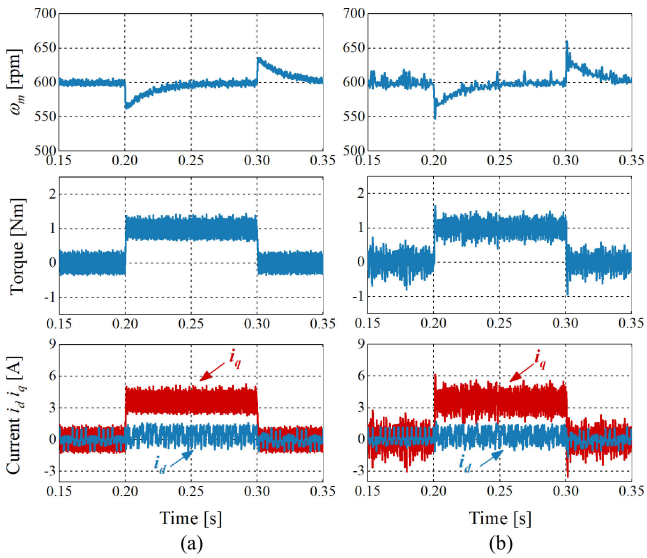

Fig. 20. Load torque change from 0 to 1 N·m, then to 0 N·m. (a) Proposed PSC-MTO. (b) Conventional PSC.

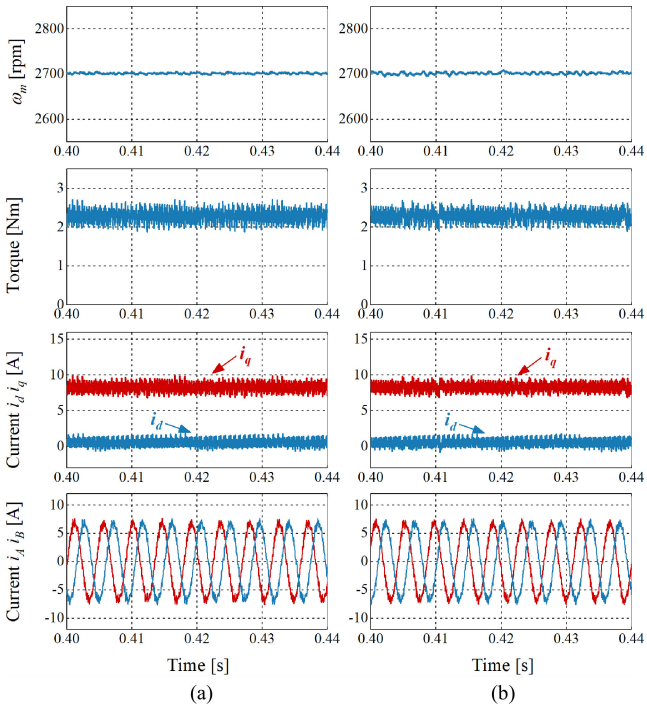

Fig. 21. Steady-state operation at speed of 90% of the rated value with 2.3-N·m nominal load torque. (a) Proposed PSC-MTO. (b) Conventional PSC.

At steady-state operation with nominal load, the torque of motor is 2.3 N·m and the speed is 90% of the rated speed. The speed, torque, *dq* currents, and phase currents of the motor for both examined methods are shown in Fig. 21. The result shows that the speeds for both methods are stable, without offset. Since the speed is steady, the speed prediction has little effect on current prediction. Both methods express the similar performance on current. The internal current controllers for the quadrature and direct stator currents track the reference well. The phase current has a sinusoidal waveform without distortion. Combined with the steady-state performance in speed reference change test,

the proposed method achieves a similar or even better overall steady-state performance over a wide speed range.

VI. Conclusion

This paper presents a cascaded PSC-MTO for a permanent-magnet synchronous motor. According to the different mechanical and electrical time constants in PMSM drives, a cascaded structure is designed to predict the speed and current, and different sampling times are assigned accordingly. In order to solve the coupling between the two-timescale models, the predictions of both slow and fast models for all the prediction instants are analyzed in detail. A linear estimation method based on virtual instants is proposed to improve the accuracy of the slow-sampling model for fast prediction instants. The data stream of the proposed method is designed based on the cascaded structure. Finally, the presented scheme is validated by experimental results with a better dynamic performance compared with conventional PSC. The developed method also exhibits the similar or even better overall steady-state performance over a wide speed range.

References

[1] P. Kakosimos and H. Abu-Rub, "Predictive speed control with short prediction horizon for permanent magnet synchronous motor drives," *IEEE Trans. Power Electron.*, vol. 33, no. 3, pp. 2740–2750, Mar. 2018.

[2] W. Tu, G. Luo, R. Zhang, Z. Chen, and R. Kennel, "Finite-control-set model predictive current control for PMSM using grey prediction," in *Proc. IEEE Energy Convers. Congr. Expo.*, Milwaukee, WI, USA, 2016, pp. 1–7.

[3] G. Luo, R. Zhang, Z. Chen, W. Tu, S. Zhang, and R. Kennel, "A novel nonlinear modeling method for permanent-magnet synchronous motors," *IEEE Trans. Ind. Electron.*, vol. 63, no. 10, pp. 6490–6498, Oct. 2016.

[4] J. Holtz, "Advanced PWM and predictive control—An overview," *IEEE Trans. Ind. Electron.*, vol. 63, no. 6, pp. 3837–3844, Jun. 2016.

[5] Y. Zhang, D. Xu, and L. Huang, "Generalized multiple-vector-based model predictive control for PMSM drives," *IEEE Trans. Ind. Electron.*, vol. 65, no. 12, pp. 9356–9366, Dec. 2018.

[6] M. Preindl and S. Bolognani, "Model predictive direct speed control with finite control set of PMSM drive systems," *IEEE Trans. Power Electron.*, vol. 28, no. 2, pp. 1007–1015, Feb. 2013.

[7] J. Richter and M. Doppelbauer, "Predictive trajectory control of permanent-magnet synchronous machines with nonlinear magnetics," *IEEE Trans. Ind. Electron.*, vol. 63, no. 6, pp. 3915–3924, Jun. 2016.

[8] F. Wang *et al.*, "Finite control set model predictive torque control of induction machine with a robust adaptive observer," *IEEE Trans. Ind. Electron.*, vol. 64, no. 4, pp. 2631–2641, Apr. 2017.

[9] A. Linder, R. Kanchan, R. Kennel, and P. Stolze, *Model-Based Predictive Control of Electric Drives*. Göttingen, Germany: Cuvillier Verlag, 2010.

[10] P. Cortes, M. Kazmierkowski, R. Kennel, D. Quevedo, and J. Rodriguez, "Predictive control in power electronics and drives," *IEEE Trans. Ind. Electron.*, vol. 55, no. 12, pp. 4312–4324, Dec. 2008.

[11] S. Vazquez, J. Rodriguez, M. Rivera, L. G. Franquelo, and M. Norambuena, "Model predictive control for power converters and drives: Advances and trends," *IEEE Trans. Ind. Electron.*, vol. 64, no. 2, pp. 935–947, Feb. 2017.

[12] T. Geyer, "Model predictive direct current control: formulation of the stator current bounds and the concept of the switching horizon," *IEEE Ind. Appl. Mag.*, vol. 18, no. 2, pp. 47–59, Mar. 2012.

[13] E. J. Fuentes, C. A. Silva, and J. I. Yuz, "Predictive speed control of a two-mass system driven by a permanent magnet synchronous motor," *IEEE Trans. Ind. Electron.*, vol. 59, no. 7, pp. 2840–2848, Jul. 2012.

[14] E. Fuentes, C. Silva, and R. Kennel, "MPC implementation of a quasitime-optimal speed control for a PMSM Drive, with inner modulated FS-MPC torque control," *IEEE Trans. Ind. Electron.*, vol. 63, no. 6, pp. 3897–3905, Jun. 2016.

[15] C. Garcia, J. Rodriguez, C. Silva, C. Rojas, P. Zanchetta, and H. Abu-Rub, "Full predictive cascaded speed and current control of an induction machine," *IEEE Trans. Energy Convers.*, vol. 31, no. 3, pp. 1059–1067, Sep. 2016.

[16] A. Darba, F. D. Belie, P. D'haese, and J. A. Melkebeek, "Improved dynamic behavior in BLDC drives using model predictive speed and current control," *IEEE Trans. Ind. Electron.*, vol. 63, no. 2, pp. 728–740, Feb. 2016.

[17] G. Stephanopoulos, O. Karsligil, and M. Dyer, "Multi-scale aspects in model-predictive control," *J. Process Control*, vol. 10, no. 2, pp. 275–282, 2000.

[18] A. Kurita *et al.*, "Multiple time-scale power system dynamic simulation," *IEEE Trans. Power Syst.*, vol. 8, no. 1, pp. 216–223, Feb. 1993.

[19] C. Garcia, C. Silva, J. Rodriguez, and P. Zanchetta, "Cascaded model predictive speed control of a permanent magnet synchronous machine," in *Proc. 42nd Annu. Conf. IEEE Ind. Electron. Soc.*, 2016, pp. 2714–2718.

[20] S. Carpiuc and C. Lazar, "Real-time multi-rate predictive cascade speed control of synchronous machines in automotive electrical traction drives," *IEEE Trans. Ind. Electron.*, vol. 63, no. 8, pp. 5133–5142, Aug. 2016.

[21] R. Errouissi, M. Ouhrouche, W. Chen, and A. M. Trzynadlowski, "Robust cascaded nonlinear predictive control of a permanent magnet synchronous motor with antiwindup compensator," *IEEE Trans. Ind. Electron.*, vol. 59, no. 8, pp. 3078–3088, Aug. 2012.

[22] C. S. Lim, E. Levi, M. Jones, N. A. Rahim, and W. P. Hew, "FCS-MPC based current control of a five-phase induction motor and its comparison with PI-PWM control," *IEEE Trans. Ind. Electron.*, vol. 61, no. 1, pp. 149–163, Jan. 2014.

[23] J. Rodriguez *et al.*, "Predictive current control of a voltage source inverter," *IEEE Trans. Ind. Electron.*, vol. 54, no. 1, pp. 495–503, Feb. 2007.

[24] T. Vyncke, S. Thielemans, and J. Melkebeek, "Finite-set model based predictive control for flying capacitor converters: Cost function design and efficient FPGA implementation," *IEEE Trans. Ind. Inform.*, vol. 9, no. 2, pp. 1113–1121, May 2013.

[25] *Zynq-7000 All Programmable SoC Technical Reference Manual*, Xilinx, Inc., San Jose, CA, USA, 2015.

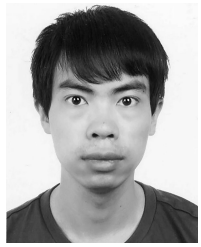

Wencong Tu (S'13) was born in Shaanxi, China, in 1988. He received the B.S. and M.S. degrees in electrical engineering from the Automation Faculty, Northwestern Polytechnical University (NPU), Xi'an, China, in 2011 and 2014, respectively. Since 2013, he has been working toward the Ph.D. degree in electrical engineering at NPU.

His research interests include predictive control for power electronics and electric drives, real-time simulation technology for electrical drive system, and application of a field-programmable gate array based digital controller.

Guangzhao Luo (M'08) received the M.S. and Ph.D. degrees in electrical engineering from Northwestern Polytechnical University (NPU), Xi'an, China, in 1998 and 2003, respectively.

From 2003 to 2004, he was a Postdoctoral Researcher with the University of Federal Defense, Munich, Germany. He is currently a Professor with NPU. He is the Vice-Director of the Rare Earth Permanent Magnet Electric Machine and Control Engineering Center, Shaanxi Province, China. His research interests include advance control theory of a permanent-magnet electrical machine, high performance control technology of a permanent-magnet synchronous motor for electric traction and electric vehicles, real-time simulation technology for electrical drive systems, and intelligence control of new energy conversion.

Dr. Luo was the recipient of the Second Prize from the China National Defense Science and Technology Progress Award in 1995 and 2011.

Zhe Chen (M'13) was born in Shanxi, China, in 1986. He received the B.S. and M.S. degrees in electrical engineering from the Automation Faculty, Northwestern Polytechnical University, Xi'an, China, in 2008 and 2011, respectively, and the Ph.D. degree from the Institute for Electrical Drive Systems and Power Electronics, Technical University of Munich, Munich, Germany, in 2016.

Since 2017, he has been an Associate Professor with Northwestern Polytechnical University. His research interests include predictive control and sensorless control for power electronics and electric drives, renewable energy systems, and application of field-programmable gate array based digital controllers.

Longran Cui was born in Henan, China, in 1993. He is currently working toward the M.S. degree with the Automation Faculty, Northwestern Polytechnical University, Xi'an, China.

His main research interests are driving and controlling of permanent-magnet synchronous motor and application of power electronic devices.

Ralph Kennel (M'89–SM'96) was born in Kaiserslautern, Germany, in 1955. He received the Diploma and the Dr.-Ing. (Ph.D.) degrees in electrical engineering from the University of Kaiserslautern, Kaiserslautern, Germany, in 1979 and 1984, respectively.

From 1983 to 1999, he worked on several positions with Robert BOSCH GmbH, Stuttgart, Germany. From 1994 to 1999, he was appointed as a Visiting Professor with the Newcastle University, Newcastle upon Tyne, U.K. From 1999 to 2008, he was a Professor in electrical machines and drives with Wuppertal University, Wuppertal, Germany. Since 2008, he has been a Professor in electrical drive systems and power electronics with the Technische Universtät München, Munich, Germany. His current research interests are sensorless control of ac drives, predictive control of power electronics, and hardware-in-the-loop systems.

Dr. Kennel is a Fellow of IET (former IEE) and a Chartered Engineer in the U.K. Within IEEE, he is a Treasurer of the Germany section as well as ECCE Global Partnership Chair of the Power Electronics Society.